# $Mn_{12}$-Acetate Complexes Studied as Single Molecules

Matthias Tombers,[a] Jennifer Meyer,[a] Jonathan Meyer,[a] Arkadiusz Lawicki,[b] Vicente Zamudio-Bayer,[b] Konstantin Hirsch,[b] J. Tobias Lau,[b, c] Bernd von Issendorff,[c] Akira Terasaki,[d] Thomas A. Schlathölter,[e] Ronnie A. Hoekstra,[e] Sebastian Schmidt,[f] Annie K. Powell,[f] Eva Kessler,[a] Marc H. Prosenc,[a] Christoph van Wüllen,[a] and Gereon Niedner-Schatteburg*[a]

*Dedicated to Helmut Baumgärtel and Wolfgang Eberhardt in recognition of their long standing devotion for the BESSY I and BESSY II synchrotron light sources.*

**Abstract:** The phenomenon of single molecule magnet (SMM) behavior of mixed valent $Mn_{12}$ coordination clusters of general formula $[Mn^{III}_8Mn^{IV}_4O_{12}(RCOO)_{16}(H_2O)_4]$ had been exemplified by bulk samples of the archetypal $[Mn^{III}_8Mn^{IV}_4O_{12}(CH_3COO)_{16}(H_2O)_4]$ **(4)** molecule, and the molecular origin of the observed magnetic behavior has found support from extensive studies on the $Mn_{12}$ system within crystalline material or on molecules attached to a variety of surfaces. Here we report the magnetic signature of the isolated cationic species $[Mn_{12}O_{12}(CH_3COO)_{15}(CH_3CN)]^+$ **(1)** by gas phase X-ray Magnetic Circular Dichroism (XMCD) spectroscopy, and we find it closely resembling that of the corresponding bulk samples. Furthermore, we report broken symmetry DFT calculations of spin densities and single ion tensors of the isolated, optimized complexes $[Mn_{12}O_{12}(CH_3COO)_{15}(CH_3CN)]^+$ **(1)**, $[Mn_{12}O_{12}(CH_3COO)_{16}]$ **(2)**, $[Mn_{12}O_{12}(CH_3COO)_{16}(H_2O)_4]$ **(3)**, and the complex in bulk geometry $[Mn^{III}_8Mn^{IV}_4O_{12}(CH_3COO)_{16}(H_2O)_4]$ **(5)**. The found magnetic fingerprints – experiment and theory alike – are of a remarkable robustness: The $Mn^{IV}_4$ core bears almost no magnetic anisotropy while the surrounding $Mn^{III}_8$ ring is highly anisotropic. These signatures are truly intrinsic properties of the $Mn_{12}$ core scaffold within all of these complexes and largely void of the environment. This likely holds irrespective of bulk packing effects.

## Introduction

Single Molecule Magnets (SMMs) are recognized as promising and novel magnetic entities which could be used in high density data storage devices[1] and for quantum computing.[2,3] SMMs are characterized by a non-zero spin state and a significant magnetic anisotropy barrier, which results in slow relaxation of magnetization.[4] The archetypal $[Mn^{III}_8Mn^{IV}_4O_{12}(CH_3COO)_{16}(H_2O)_4]$ **(4)** coordination cluster[5,6] has a non-zero spin ground state, which arises from an effective antiferromagnetic (spin antiparallel) coupling between an outer ring of 8 ferromagnetically (spin parallel) coupled $Mn^{III}$ ions ($S = 16$) and an inner distorted tetrahedron of 4 ferromagnetically arranged $Mn^{IV}$ ($S = 6$) ions (Scheme 1) resulting in a net spin of $S = 10$.[7] Uniaxial magnetic anisotropy is induced by the Jahn-Teller distorted $Mn^{III}$ sites, which leads to a barrier for spin

[a] Dr. M. Tombers, Jun. Prof. Dr. J. Meyer, Dr. J. Meyer, Dr. E. Kessler, Dr. M. H. Prosenc, Prof. Dr. C. van Wüllen, Prof. Dr. Dr. G. Niedner-Schatteburg
Fachbereich Chemie and Forschungszentrum OPTIMAS
Technische Universität Kaiserslautern (TUK)
67663 Kaiserslautern (Germany)
E-mail: gns@chemie.uni-kl.de

[b] Dr. A. Lawicki, Dr. V. Zamudio-Bayer, Dr. K. Hirsch, Prof. Dr. J. T. Lau
Abteilung für Hochempfindliche Röntgenspektroskopie
Helmholtz Zentrum Berlin für Materialien und Energie
12489 Berlin-Adlershof (Germany)

[c] Prof. Dr. J. T. Lau, Prof. Dr. B. von Issendorff
Physikalisches Institut
Albert-Ludwigs-Universität Freiburg
79104 Freiburg (Germany)

[d] Prof. Dr. A. Terasaki
Department of Chemistry
Kyushu University
Fukuoka 819-0395 (Japan)

[e] Prof. Dr. T. A. Schlathölter, Prof. Dr. R. A. Hoekstra
Zernike Institute for Advanced Materials
University of Groningen
Groningen (Netherlands)

[f] Dr. S. Schmidt, Prof. Dr. A. K. Powell
Institut für Anorganische Chemie
Karlsruher Institut für Technologie (KIT)
Karlsruhe (Germany)

Supporting information for this article is available on the WWW under https://doi.org/10.1002/chem.202102592

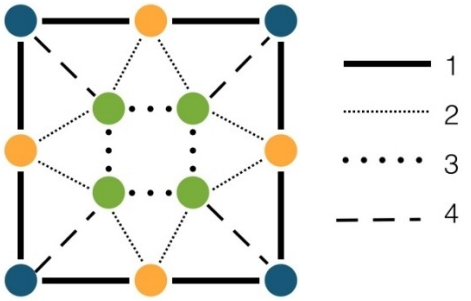


**Scheme 1.** 2D schematic depiction of the Mn–Mn scaffold (1–4, see Supporting Information Tables S1 and S2) for the three kinds of Mn atoms with different coordination (blue, orange and green spheres) within the 3D $[Mn_{12}O_{12}(CH_3COO)_{16}]$ complexes. Previous, widely accepted analysis assigns the oxidation state III to all of the four blue and four orange Mn atoms, which from an outer ring, and the oxidation state IV to the central four green Mn atoms, which form an inner core.[6]

reversal between the $M_S = \pm 10$ ground states as evidenced, for example, by low-temperature hysteresis in magnetization measurements.[6] The molecular origin of the observed magnetic behavior finds support from extensive studies on the $Mn_{12}$ system[8] within crystalline material[9,10] or on molecules attached to a variety of surfaces.[11–14] It was found, for example, that the magnetic relaxation exhibits Arrhenius like behavior with an effective anisotropy energy barrier $\Delta E/k_B = 61K$ (or 45 $cm^{-1}$)[15,16] and a prefactor of $\tau_0 = 2.1 \bullet 10^{-7}s$, leading to a magnetic relaxation time of approximately 250 *ns* at room temperature.[17] At low temperatures deviations from this behavior occur, which are due to quantum tunnelling of the magnetization.[18–20] Further properties of this coordination complex, for example, the magnetic spin ground state value S = 10, have been extensively characterized by SQUID magnetometry,[9] EPR spectroscopy[6] and X-ray Magnetic Circular Dichroism (XMCD) spectroscopy measurements of bulk samples.[5,6]

Based on these results it is generally assumed that the magnetic moment and the anisotropy energy are intrinsic properties of the isolated, single molecules and do not result from any bulk effect like long range magnetic ordering. The environment of the molecules can have an influence, though,[8] which is most clearly seen in the case of surface deposited molecules, where charge transfer from the surface to the molecule may lead to a partial reduction of the $Mn^{III}$ ions and a resulting strong change of the magnetic properties of the molecule.[11,21]

In order to elucidate its intrinsic magnetic behavior, we have performed XMCD studies of a gas phase ionic $[Mn_{12}O_{12}(CH_3COO)_{15}(CH_3CN)]^+$ complex (abbreviated as $[Mn_{12}ac]^+$ **(1)**) when isolated in a cryogenic ion trap.[22–24] We compare our data with those from previous XMCD studies on related bulk phase neutral complexes $[Mn^{III}{}_8Mn^{IV}{}_4O_{12}(CH_3COO)_{16}(H_2O)_4]$[8] (abbreviated as $[Mn_{12}ac](H_2O)_4{}^{(bulk)}$ **(4)**) and others, and we discuss the like and unlike features found. We further continue and extend a previous study[25] by reporting broken symmetry DFT calculations of the isolated complexes $[Mn_{12}ac]^+$ **(1)**, $[Mn_{12}O_{12}(CH_3COO)_{16}]$ (abbreviated $[Mn_{12}ac]$ **(2)**), $[Mn_{12}O_{12}(CH_3COO)_{16}(H_2O)_4]$, (abbreviated $[Mn_{12}ac](H_2O)_4$ **(3)**, and isolated $[Mn^{III}{}_8Mn^{IV}{}_4O_{12}(CH_3COO)_{16}(H_2O)_4]$ in bulk geometry (abbreviated $[Mn_{12}ac](H_2O)_4{}^{(bulk\ geo)}$ **(5)**), and we discuss the found magnetic fingerprints of these species (Table 1) – experiment and theory alike – in terms of their intrinsic robustness.

## Experimental and Computational Details

**XAS and XMCD experiments**. Gas phase XMCD spectra of $[Mn_{12}O_{12}(CH_3COO)_{15}(CH_3CN)]^+$ complex, in short $[Mn_{12}ac]^+$ **(1)**, were obtained through measurement of the X-ray Absorption Spectra (XAS) of left (lcp,-) and right (rcp,+) handed circularly polarized synchrotron radiation.[22,24,26] Subtraction of these XAS spectra unravels any dichroic effect known as XMCD spectrum. We used the combination of an Electro Spray Ionization source (ESI) with the Ion Trap end-station operated at the UE52-PGM beamline at the BESSY II (Helmholtz Zentrum Berlin) synchrotron facility.[22,27] The Ion Trap end-station has proven suitable to record XMCD spectra of isolated species in the gas phase during the investigation of magnetic moments of isolated transition metal clusters[22] and complexes.[27] A detailed description of the setup is given elsewhere.[28] In brief, after generating isolated $[Mn_{12}ac]^+$ **(1)** from solution in the electrospray ion source the investigated ion is mass selected in a quadrupole mass filter and is transferred into a liquid helium cooled linear quadrupole ion trap. The ion $[Mn_{12}ac]^+$ **(1)** is formed by replacing a negatively charged acetate ligand with a neutral acetonitrile solvent molecule. The four coordinating water molecules present in the crystal structure cannot be observed in the gas phase mass spectrum. The quadrupole ion trap is located within the high field region of a superconducting solenoid ($B_{ext}$ = 5 T). The magnetic field axis, the trap axis and X-ray beam path are in a parallel arrangement. The ion trap is cooled to a temperature of 3–4 K, and the molecular ions are thermalized by a constant flow of precooled He-buffer gas to a temperature of roughly 10–30 K.[26] The cooled ions are irradiated for up to 10 seconds with circularly polarized X-ray radiation in the range of 630–665 eV which covers the manganese $L_{2,3}$-edges. After photon absorption, the ions start to fragment following multiple consecutive Auger processes. An in line reflectron time of flight mass spectrometer serves to record the resulting fragment mass spectra. Ions are constantly refilled from the cluster source and analyzed after irradiation periodically at a repetition rate of 20 Hz. With this Partial Ion Yield (PIY) action spectroscopy we gain X-ray absorption spectra by recording the amount of fragment ions as a function of X-ray energy and helicity. The spectra were recorded with a spectral resolution of 370 meV at 643 eV and an increment size of 200 meV, averaging over multiple scans across the spectral range.

All spectra of the present study were recorded at the highest possible magnetic field and lowest achievable trap temperature to ensure significant magnetization of the free ions. The structural alignment of the of $[Mn_{12}ac]^+$ **(1)** samples within the Ion Trap end-station is evaluated and put into perspective, see Text S6 and Figures S7 through S11 in the Supporting Information. Due to the low ion density within the ion trap, magnetization curves by either scanning magnetic field or trap temperature were beyond the scope of the current explorative study. The quite new conduct of gas phase XMCD experiments is by now a well-established procedure at the Ion Trap end-station at the BESSY II synchrotron in Berlin, and it was also conducted at the GAMBIT setup before.[22–24] Nevertheless, experiments remain challenging which is due to the low density of the target that merely comprises of a cloud of guided ions.

**Data analysis**. Onsets of resonant absorptions at the $L_2$ and $L_3$ edge and uncertainties were determined as reported before,[22,26] and the obtained data were normalized to the photon flux of the beamline. The linear absorption spectra (Figure 1b) originate from an average of the X-ray absorption spectra for parallel ($\sigma^-$) and antiparallel ($\sigma^+$) alignment of photon helicity with respect to the magnetization axis. These spectra were corrected for their direct ionization background by subtraction of a two-step function,[29] and they were subsequently normalized to the maximum intensity of the $L_3$ absorption edge. Eventually, we scaled our XMCD spectrum by a factor of 0.98 to match the maximum of the positive dichroic signal at the $L_3$ edge of the bulk spectrum (Figure 2).

**Quantum Chemical calculations**. All geometry optimizations were performed using density functional theory, using the TURBOMOLE 6.5 package.[30,31] We chose the hybrid exchange correlation functional PBE0,[32] the basis set def2-TZVP,[33,34] and the D3 dispersion correction.[35] No relativistic effects were included in the geometry optimizations, and the geometry optimizations were done for the broken-symmetry configuration where the number of alpha-spin electron exceeds the number of beta-spin electrons by 20. For $[Mn_{12}ac](H_2O)_4^{(bulk\ geo)}$ **(5)**, only the hydrogen positions were optimized while the non-hydrogen positions were taken from the experimental X-ray geometry. For the other three species, a full geometry optimization of all atomic positions was done. We investigated different high (HS) and low spin (LS) states with broken symmetry configurations, thereby checking for ferromagnetic and antiferromagnetic coupling between the outer $Mn^{III}{}_8$ ring and the inner $Mn^{IV}{}_4$ core. This was done for the neutral $[Mn_{12}ac](H_2O)_4^{(bulk\ geo)}$ **(5)** in the known bulk geometry without structural relaxation of the non-hydrogen atoms, and for the cationic $[Mn_{12}ac]^+$ **(1)** species with full structural relaxation. For details on computed geometries refer to Supporting Information Figure S1 and Supporting Information Tables S1-S4, which also encompass further results on fully optimized $[Mn_{12}ac]$ **(2)** and $[Mn_{12}ac](H_2O)_4$ **(3)** species.

**Calculation of single ion tensors**. The microscopic origin of the zero-field splitting or magnetic anisotropy is the spin-orbit coupling and spin-dipolar coupling, both these contributions are calculated by leading-order perturbation theory starting from scalar-relativistic calculations. While the spin-orbit contribution is a second order (response) property, the spin-dipolar contribution is a first-order property, that is, the expectation value of the electron-electron spin-dipolar interaction with the scalar-relativistic wave function. The calculation of the zero field splitting tensors was performed with our in-house variant of the TURBOMOLE program.[36] The quasirelativistic ZORA operator[37,38] provides the scalar and spin-orbit parts of the Hamiltonian, and the spin-dipolar and spin-orbit contributions to the zero field splitting tensors were calculated as described in Ref.[25,39] The ZORA calculations were performed using the PBE0 exchange-correlation functional[32] and TZVP basis sets,[40] where the Mn TZVP basis sets has been recontracted for use with the ZORA Hamiltonian. The breakdown of the global zero field splitting tensor into single-ion contributions was performed as described in Ref.[41] For the spin-orbit part, we use localized occupied orbitals to decompose the magnetic anisotropy into single-ion contributions, for the spin-dipolar part we use a real-space cut-off of 2 Bohr (105.8 pm), that applied to the distance of a spin center and the center of gravity of the product of basic functions. In principle one then has to average over the results from all possible broken symmetry configurations, but in the present cases, the single-ion tensors extracted from different broken-symmetry configurations differ only marginally, which also indicates that pseudo dipolar exchange interactions are negligible.

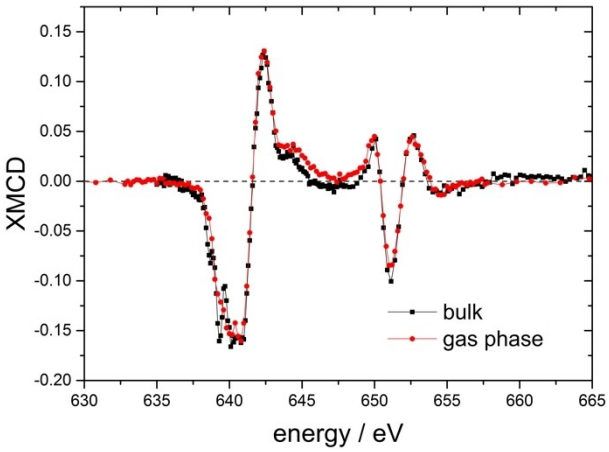


**Figure 2.** Gas phase XMCD spectrum of $[Mn_{12}ac]^+$ **(1)** at $T_{trap} = 15$ K and $B_{ext} = 5$ T (this work, red circles) and solid-state data on $[Mn_{12}ac](H_2O)_4^{(bulk)}$ **(4)** by Mannini et al.[11] (black squares). The minor differences around 639 eV are discussed in the context of the XAS data; see text for details. The residuum of both spectra almost diminishes otherwise.

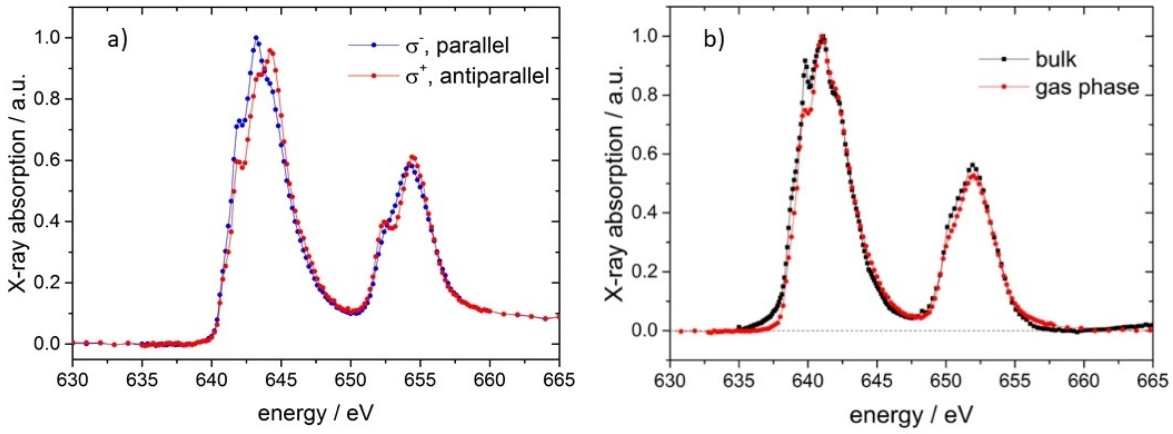


**Figure 1.** Gas phase X-ray absorption spectra at the Mn $L_3$ and $L_2$ absorption edge of **a)** $[Mn_{12}ac]^+$ **(1)** recorded with parallel ($\sigma^-$, blue) and antiparallel ($\sigma^+$, red) alignment of X-ray photon helicity and magnetization ($T_{trap} = 15$ K and $B_{ext} = 5$ T), **b)** the linear X-ray absorption spectra (average of $\sigma^-$ and $\sigma^+$) of this work (red) and the bulk phase data on $[Mn_{12}ac](H_2O)_4^{(bulk)}$ **(4)** by Mannini et al. (black).[14]

## Results and Discussion

**Results of gas phase XMCD experiments**. We recorded X-ray absorption spectra of $[Mn_{12}ac]^+$ **(1)** in the gas-phase using circularly polarized synchrotron radiation (Figure 1a), and the chosen experimental conditions ($T_{trap} = 15$ K and $B_{ext} = 5$ T) are sufficient to achieve a magnetization of 82%. Absorption edges were assigned to $L_3$ at 641 eV and $L_2$ at 655 eV, corresponding to the $2p_{3/2} \rightarrow 3d$ and $2p_{1/2} \rightarrow 3d$ resonant excitations (Figure 1a). Both excitation bands are structured due to the presence of two formal oxidation states of the Mn-atoms within the $Mn_{12}$-complex.

The averaged XAS spectrum, corresponding to linear polarization XAS, closely resembles the solid-state XAS of $[Mn_{12}ac](H_2O)_4^{(bulk)}$ **(4)** (Figure 1b). Both spectra agree on both absorption edges in almost quantitative manner. We observe in the gas phase spectrum a reduction of the absorption peak at 639.8 eV which is more pronounced in the solid-state spectrum. This peak was assigned by Mannini et al.[11,26] to the absorption of Mn(II),[42] and it might arise either from charge transfer with the conductive surface as predicted before[43] or from some radiation damage of about 5%. The present study utilizes samples in the form of trapped ions which are continuously renewed such that radiation damage may not accumulate. Moreover, the sample preparation involves mass selection and thus a determination of mass to charge ratio prior to irradiation, which renders initial redox processes impossible. Finally, samples of this study are isolated and not in contact with any surface.

From the lcp and rcp X-ray absorption spectra we deduce the XMCD spectrum (Figure 2), which reveals a complicated pattern of several positive and negative dichroic effects within the $L_2$ and $L_3$ bands that originate from individual contributions of $Mn^{III}$ and $Mn^{IV}$ species superimposing. The gas phase XMCD spectrum of $[Mn_{12}ac]^+$ **(1)** agrees well with the previously reported XMCD spectrum of crystalline $[Mn_{12}ac](H_2O)_4^{(bulk)}$ **(4)**.[11,44] For comparison to further bulk spectra see Supporting Information Figure S3. Note, that variations around 638 eV amongst the bulk spectra are larger than the deviation of the present gas phase and the depicted bulk spectrum. Further minor differences in the XAS and XMCD spectra of bulk and gas phase samples might arise from small changes in ligand fields, for example due to the four coordinating water molecules of the bulk sample $[Mn_{12}ac](H_2O)_4^{(bulk)}$ **(4)**, which are absent in investigated gas phase samples of $[Mn_{12}ac]^+$ **(1)**.

The magnitude of the dichroic effect observed in the XMCD spectrum indicates a significant spin moment of $[Mn_{12}ac]^+$ **(1)** (Figure 2), which is in accordance with the reported spin state $S = 10$ of $[Mn_{12}ac](H_2O)_4^{(bulk)}$ **(4)**. Application of the orbital moment sum rule[45] yields a total orbital magnetic moment of $m_L = 1.4 \pm 1.7\ \mu_B$, which is zero within obtained error bars, and compatible with the small negative orbital magnetic moment of about $-0.5\ \mu_B$ from XMCD and ESR studies of $[Mn_{12}ac](H_2O)_4^{(bulk)}$ **(4)** in solid state.[6]

All of the above observed minor differences do not detract from the fact that the magnetic signatures of bulk and gas phase spectra are essentially identical. This proves that XAS/XMCD spectral fingerprints are governed by intrinsic properties of the $[Mn_{12}ac]$ complexes. Nevertheless one has to keep in mind that our XMCD study has been performed on a $[Mn_{12}ac]^+$ complex cation in the gas phase, where an anionic acetate ligand of $[Mn_{12}ac](H_2O)_4^{(bulk)}$ is exchanged for a neutral acetonitrile solvent molecule, and no water ligands are present. In principle, such auxiliary ligands and other crystal packing effects could contribute to the observed spectra, which poses the fundamental question of the $[Mn_{12}ac]$ scaffolds magnetic robustness, and whether the observed spin properties of $[Mn_{12}ac]$-type complexes are influenced by the local environment. We will further elucidate these questions by the subsequent quantum chemical modelling.

**Broken symmetry DFT modelling and single ion tensors**. The SMM behavior of a polynuclear complex is governed by the zero field splitting of the individual spin centers and by their interactions. We chose for our modelling the isolated complexes $[Mn^{III}_8Mn^{IV}_4O_{12}(CH_3COO)_{16}(H_2O)_4]$ in the bulk phase geometry – labelled $[Mn_{12}ac](H_2O)_4^{(bulk\ geo)}$ **(5)**, isolated $[Mn_{12}ac]^+$ **(1)**, fully optimized $[Mn_{12}ac]$ **(2)**, and fully relaxed $[Mn_{12}ac](H_2O)_4$ **(3)**. We performed broken symmetry density functional theory (BS-DFT) calculations (See Experimental section) on all of these species. We calculated both the high-spin (HS) configuration where all 44 unpaired electrons are spin-up ($<S_z> = 22$) and a low-spin (LS) configuration with $<S_z> = 10$. In the latter case, the 12 unpaired electrons on the four central $Mn^{IV}$ ions are spin-down and the 32 unpaired electrons at the eight outer $Mn^{III}$ ions are spin-up. The LS configuration turned out more stable, and we obtained its spin density as depicted (Figure 3). In the cases of both $[Mn_{12}ac](H_2O)_4^{(bulk\ geo)}$ **(5)** and $[Mn_{12}ac]^+$ **(1)**, the spin density leaks from the Mn sites to the oxygen atoms of the $Mn_{12}O_{12}$ core in a very similar way, and very little spin density is found either on the acetate ligands or on the sole acetonitrile ligand. Transforming $[Mn_{12}ac](H_2O)_4^{(bulk\ geo)}$ **(5)** into $[Mn_{12}ac]^+$ **(1)** thus leaves spin densities – and even more so the geometries of the $Mn_{12}O_{12}$ cores – virtually unchanged (see Supporting Information Tables S1, S2 and S3). This holds as well for the spin densities and scaffold geometries of $[Mn_{12}ac]$ **(2)** and $[Mn_{12}ac](H_2O)_4$ **(3)** complexes (see Supporting Information Figure S4, and Tables S1, S2, and S3). The calculated energy differences between the HS and LS configurations of all four species are almost the same (on the order of 30 kJ mol$^{-1}$, see Supporting Information Table S4). This indicates that the isotropic exchange coupling between the spin centers is not much different in all calculated complexes and the nature of the spin ground state should be the same.

Furthermore, we extracted the single-ion tensors for all four species, and we found that they are only marginally affected by the structural changes. These tensors reveal local anisotropy axes', which signify the easy axis direction and the magnitude of the single-ion D value, of each of the 12 Mn centers, as indicated for $[Mn_{12}ac](H_2O)_4^{(bulk\ geo)}$ **(5)** and $[Mn_{12}ac]^+$ **(1)** by arrows in Figure 4 (see the Supporting Information, Figure S5 for the results on $[Mn_{12}ac]$ **(2)** and $[Mn_{12}ac](H_2O)_4$ **(3)**. All of the eight outer $Mn^{III}$ ions reveal much parallel anisotropy axes', and the contributions of the four nearly isotropic $Mn^{IV}$ ions in the inner core are smaller by an order of magnitude and thus not

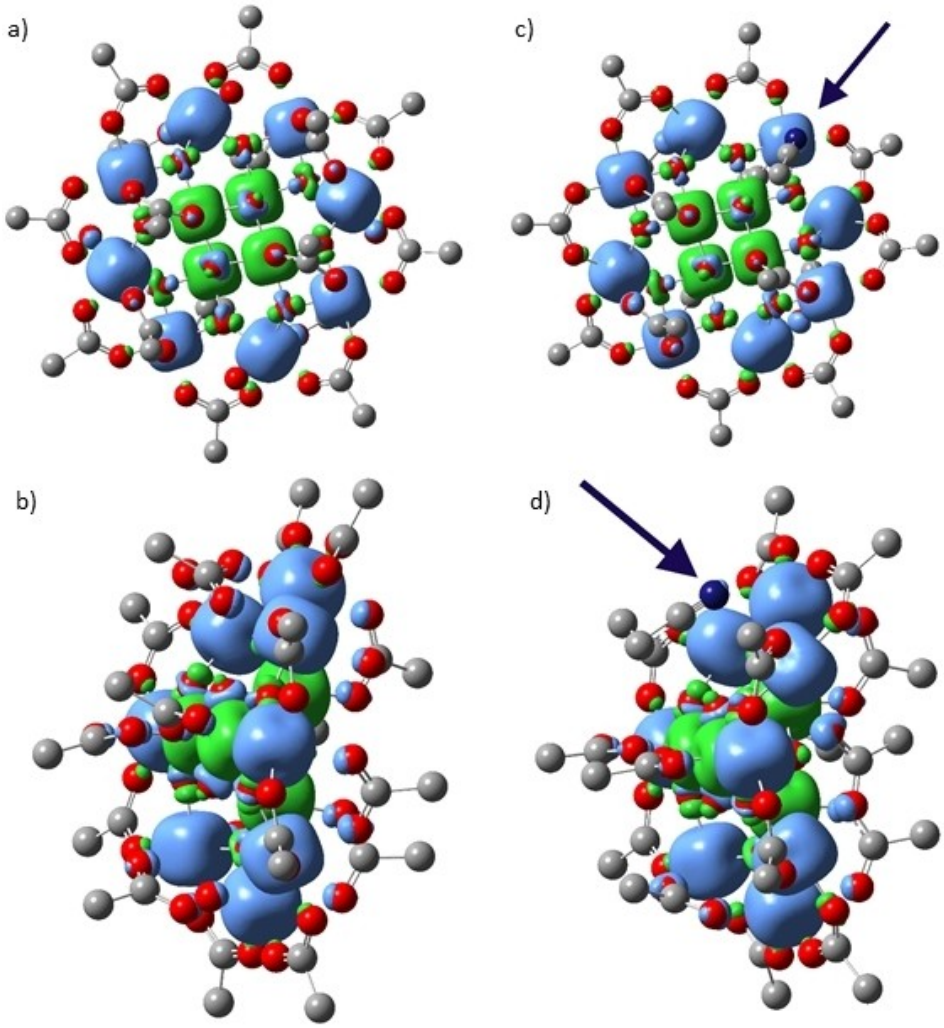


**Figure 3.** Spin density plots by broken symmetry – DFT calculations of α (light blue) and β (green) spin densities in $[Mn_{12}ac](H_2O)_4^{(bulk\ geo)}$ **(5)**, (a) and (b), and in $[Mn_{12}ac]^+$ **(1)**, (c) and (d); H-atoms omitted for clarity; (b) and (d) providing side on views of (a) and (c). Identify the sole $CH_3CN$ ligand by its dark blue N atom in the top right of (c) and in the top left of (d), respectively, and as emphasized by the arrows. Spin density plots of $[Mn_{12}ac]$ **(2)** and $[Mn_{12}ac](H_2O)_4$ **(3)** complexes are virtually identical (see Supporting Information Figure S4).

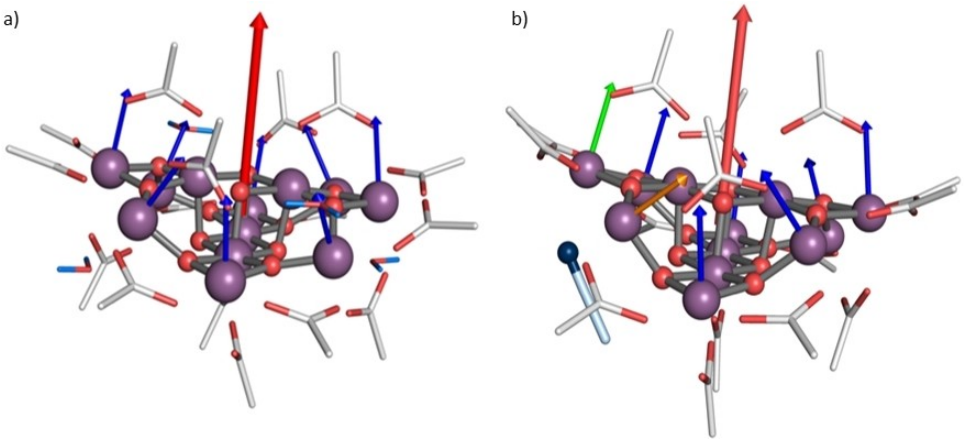


**Figure 4.** Single ion magnetic anisotropy tensors in (a) $[Mn_{12}ac](H_2O)_4^{(bulk\ geo)}$ **(5)** and (b) $[Mn_{12}ac]^+$ **(1)** . Blue vectors indicate the largest eigenvectors of the single ion tensors at each Mn atom, with light green and orange vectors identifying those tensors which are directly affected by the ligand swap of an acetonitrile for an acetate. The red arrow indicates the direction of the eigenvector sum which is the easy axis of magnetization. Note, that the inner four Mn centers do not contribute; their individual magnetic anisotropy is vanishingly small.

discernible; for their values see Tables S5 and S6 in the Supporting Information. The anisotropic interactions between the spin centers are dominated by two-center spin-dipolar couplings which depend on the scaffolds geometry and are thus also similar for $[Mn_{12}ac](H_2O)_4^{(bulk\ geo)}$ **(5)** and $[Mn_{12}ac]^+$ **(1)** species, and for $[Mn_{12}ac]$ **(2)** and $[Mn_{12}ac](H_2O)_4$ **(3)** as well.

Comparing $[Mn_{12}ac](H_2O)_4^{(bulk\ geo)}$ **(5)** and $[Mn_{12}ac]^+$ **(1)**, we see changes in the magnitude of the single-ion magnetic anisotropy of about 10% (see Figure 4, and Tables S5-S8), and no reorientation of single ion tensors but the one of the $Mn^{III}$ center in $[Mn_{12}ac]^+$ **(1)** that comes with one coordinating ligand less (orange arrow). For the eight peripheral $Mn^{III}$ centers of the outer ring, the main local anisotropy axis always aligns with the "long" axis of the local tetragonally distorted environment – but for the orange one. However, this tilt of the orange vector has a negligible effect on the orientation of the easy magnetization axis (red arrows).

Note that in the three neutral $Mn_{12}$-complexes the single-ion tensors have non-zero but small rhombicity. Because of the high symmetry of these three complexes the total zero field splitting tensor is axial anyway. In $[Mn_{12}ac]^+$ **(1)**, a small rhombicity of the (overall) zero field splitting tensor has to be expected due to the lower symmetry, and in this regard it is inferior to the high symmetry $Mn_{12}$-complexes. Nevertheless, it served well to elucidate the robustness of the $Mn_{12}$ scaffold.

The computational results thus suggest that removal of the water ligands and replacing one acetate by an acetonitrile molecule should neither alter the isotropic coupling between the Mn centers as well as their single-ion magnetic anisotropy; together this suggests very similar spin textures – in accord with the conclusions from experiment.

## Conclusions

We reported the XAS and XMCD spectra of isolated cationic $[Mn_{12}]$ acetate complexes in the gas phase. The observed spectral characteristics of the $L_2$ and $L_3$ edges agree with the reported data for bulk samples. Density functional theory calculations predict single ion zero field splitting tensors which help us to conclude that structural changes of the ligand environment have only small influence on the magnetic texture of the $Mn_{12}$ core: While there is a strong local influence of a ligand substitution as shown by our DFT calculations, the overall properties are preserved as shown by the close correspondence of our XAS/XMCD spectra of isolated complexes to those of various bulk samples. The $Mn_{12}$ core scaffold is quite robust, and its observed single molecule magnet (SMM) properties are intrinsic properties which prevail in isolated complexes as well as in bulk samples.

We thus confirm that the reported bulk studies on the Single Molecule Magnet $[Mn_{12}ac](H_2O)_4^{(bulk)}$ **(4)** addresses the single molecule characteristics even when these are organized into crystalline arrays. This opens the prospect that future studies can use the results of gas phase measurements as a benchmark for both solid state and surface deposited systems by making it possible to clearly identify additional intermolecular interactions as well as couplings to an environment.

## *Acknowledgements*

This work was supported through the DFG funded transregional collaborative research center SFB TRR 88 "3MET.de" and the BMBF grant BMBF-05K13Vf2. We gratefully acknowledge the financial support and allocation of X-ray beam time at the UE52 – PGM beamline from HZB at the BESSY II synchrotron radiation facility. We thank the Toyota Technological Institute for providing the superconducting magnet for the conducted experiments. We thank R. Sessoli for providing the bulk phase data shown in Figures 1b and 2, and we thank Joachim Hewer for valuable discussions. Finally, we want to thank the reviewers for valuable comments. Open Access funding enabled and organized by Projekt DEAL.

## Conflict of Interest

The authors declare no conflict of interest.

**Keywords:** broken symmetry DFT modelling · gaseous ions · single ion magnetic anisotropy tensors · single molecule magnets · XMCD spectroscopy · X-ray spectroscopy

[1] K. V. Raman, A. M. Kamerbeek, A. Mukherjee, N. Atodiresei, T. K. Sen, P. Lazic, V. Caciuc, R. Michel, D. Stalke, S. K. Mandal, S. Blugel, M. Munzenberg, J. S. Moodera, *Nature* **2013**, *493*, 509–513.
[2] M. N. Leuenberger, D. Loss, *Nature* **2001**, *410*, 789–793.
[3] M. Shiddiq, D. Komijani, Y. Duan, A. Gaita-Arino, E. Coronado, S. Hill, *Nature* **2016**, *531*, 348-++.
[4] J. Villain, F. Hartman-Boutron, R. Sessoli, A. Rettori, *Europhys. Lett.* **1994**, *27*, 159.
[5] T. Lis, *Acta Crystallogr. Sect. B* **1980**, *36*, 2042–2046.
[6] D. Gatteschi, A. L. Barra, A. Caneschi, A. Cornia, R. Sessoli, L. Sorace, *Coord. Chem. Rev.* **2006**, *250*, 1514–1529.
[7] R. Sessoli, D. Gatteschi, A. Caneschi, M. Novak, *Nature* **1993**, *365*.
[8] R. Bagai, G. Christou, *Chem. Soc. Rev.* **2009**, *38*, 1011–1026.
[9] G. Rogez, B. Donnio, E. Terazzi, J. L. Gallani, J. P. Kappler, J. P. Bucher, M. Drillon, *Adv. Mater.* **2009**, *21*, 4323–4333.
[10] J. H. Kim, S. C. Wi, J. S. Kang, D.-Y. Jung, S. W. Han, K. H. Kim, *J. Magn. Magn. Mater.* **2004**, *272–276, Supporting Information*, E735–E736.
[11] M. Mannini, P. Sainctavit, R. Sessoli, C. C. d Moulin, F. Pineider, M.-A. Arrio, A. Cornia, D. Gatteschi, *Chem. Eur. J.* **2008**, *14*, 7530–7535.
[12] P. Ghigna, A. Campana, A. Lascialfari, A. Caneschi, D. Gatteschi, A. Tagliaferri, F. Borgatti, *Phys. Rev. B* **2001**, *64*.
[13] A. Saywell, G. Magnano, C. J. Satterley, L. M. A. Perdigão, A. J. Britton, N. Taleb, M. del Carmen Giménez-López, N. R. Champness, J. N. O'Shea, P. H. Beton, *Nat. Commun.* **2010**, *1*, 75.
[14] M. Mannini, F. Pineider, C. Danieli, F. Totti, L. Sorace, P. Sainctavit, M. A. Arrio, E. Otero, L. Joly, J. C. Cezar, A. Cornia, R. Sessoli, *Nature* **2010**, *468*, 417–421.
[15] A. Caneschi, D. Gatteschi, R. Sessoli, A. L. Barra, L. C. Brunel, M. Guillot, *J. Am. Chem. Soc.* **1991**, *113*, 5873–5874.
[16] T. Glaser, *Chem. Commun.* **2011**, *47*, 116–130.
[17] A. Gomes, M. Novak, R. Sessoli, A. Caneschi, D. Gatteschi, *Phys. Rev. B* **1998**, *57*, 5021.
[18] L. Thomas, F. Lionti, R. Ballou, D. Gatteschi, R. Sessoli, B. Barbara, *Nature* **1996**, *383*, 145–147.
[19] D. Gatteschi, R. Sessoli, *Angew. Chem. Int. Ed.* **2003**, *42*, 268–297; *Angew. Chem.* **2003**, *115*, 278–309.

[20] J. R. Friedmann, in: *Resonant magnetization tunneling in molecular magnets*, (Eds.: J. R. Friedmann, S. Han), Nova Science, Hauppauge, **2003**, p. 179.
[21] M. Mannini, F. Pineider, P. Sainctavit, C. C. D. Moulin, M. A. Arrio, A. Cornia, D. Gatteschi, R. Sessoli, *Europ. Phys. J. Special Top.* **2009**, *169*, 167–173. European Physical Journal Special Topics is the full title of this journal, and the reference is correct
[22] M. Niemeyer, K. Hirsch, V. Zamudio-Bayer, A. Langenberg, M. Vogel, M. Kossick, C. Ebrecht, K. Egashira, A. Terasaki, T. Moeller, B. V. Issendorff, J. T. Lau, *Phys. Rev. Lett.* **2012**, *108*.
[23] S. Peredkov, M. Neeb, W. Eberhardt, J. Meyer, M. Tombers, H. Kampschulte, G. Niedner-Schatteburg, *Phys. Rev. Lett.* **2011**, *107*.
[24] J. Meyer, M. Tombers, C. van Wüllen, G. Niedner-Schatteburg, S. Peredkov, W. Eberhardt, M. Neeb, S. Palutke, M. Martins, W. Wurth, *J. Chem. Phys.* **2015**, *143*, 104302.
[25] C. van Wüllen, *J. Chem. Phys.* **2009**, *130*, 194109.
[26] A. Langenberg, K. Hirsch, A. Lawicki, V. Zamudio-Bayer, M. Niemeyer, P. Chmiela, B. Langbehn, A. Terasaki, B. V. Issendorff, J. T. Lau, *Phys. Rev. B* **2014**, *90*.
[27] S. T. Akin, V. Zamudio-Bayer, K. Duanmu, G. Leistner, K. Hirsch, C. Bülow, A. Ławicki, A. Terasaki, B. von Issendorff, D. G. Truhlar, J. T. Lau, M. A. Duncan, *J. Phys. Chem. Lett.* **2016**, *7*, 4568–4575.
[28] K. Hirsch, J. T. Lau, P. Klar, A. Langenberg, J. Probst, J. Rittmann, M. Vogel, V. Zamudio-Bayer, T. Moller, B. von Issendorff, *J. Phys. B* **2009**, *42*, 154029.
[29] V. Zamudio-Bayer, K. Hirsch, A. Langenberg, M. Kossick, A. Ławicki, A. Terasaki, B. v Issendorff, J. T. Lau, *J. Chem. Phys.* **2015**, *142*, 234301.
[30] TURBOMOLE V6.5 2013, http://www.turbomole.com.
[31] O. Treutler, R. Ahlrichs, *J. Chem. Phys.* **1995**, *102*, 346–354.
[32] C. Adamo, V. Barone, *J. Chem. Phys.* **1999**, *110*, 6158–6170.
[33] F. Weigend, R. Ahlrichs, *Phys. Chem. Chem. Phys.* **2005**, *7*, 3297–3305.
[34] F. Weigend, M. Häser, H. Patzelt, R. Ahlrichs, *Chem. Phys. Lett.* **1998**, *294*, 143–152.
[35] S. Grimme, J. Antony, S. Ehrlich, H. Krieg, *J. Chem. Phys.* **2010**, *132*, 154104.
[36] C. van Wüllen, *Chem. Phys. Lett.* **1994**, *219*, 8–14.
[37] E. v Lenthe, E. J. Baerends, J. G. Snijders, *J. Chem. Phys.* **1993**, *99*, 4597–4610.
[38] C. van Wüllen, *J. Chem. Phys.* **1998**, *109*, 392–399.
[39] S. Schmitt, P. Jost, C. van Wüllen, *J. Chem. Phys.* **2011**, *134*, 194113.
[40] A. Schäfer, C. Huber, R. Ahlrichs, *J. Chem. Phys.* **1994**, *100*, 5829–5835.
[41] E. M. V. Kessler, S. Schmitt, C. van Wüllen, *J. Chem. Phys.* **2013**, *139*.
[42] H. Wang, C. Bryant, M. LeGros, X. Wang, S. P. Cramer, *J. Phys. Chem. A* **2012**, *116*, 10082–10089.
[43] S. Barraza-Lopez, M. C. Avery, K. Park, *Phys. Rev. B* **2007**, *76*, 224413.
[44] K. Hirsch, V. Zamudio-Bayer, F. Ameseder, A. Langenberg, J. Rittmann, M. Vogel, T. Moeller, B. von Issendorff, J. T. Lau, *Phys. Rev. A* **2012**, *85*.
[45] B. T. Thole, P. Carra, F. Sette, G. Vanderlaan, *Phys. Rev. Lett.* **1992**, *68*, 1943–1946.

Manuscript received: July 16, 2021
Accepted manuscript online: November 21, 2021
Version of record online: December 8, 2021